Prediction of alloy precipitate shapes from first principles

2001 Europhys. Lett. 55 33

(http://iopscience.iop.org/0295-5075/55/1/033)

EUROPHYSICS LETTERS 1 July 2001

Europhys. Lett., **55** (1), pp. 33–39 (2001)

Prediction of alloy precipitate shapes from first principles

S. Müller[1](*), C. Wolverton[2], L.-W. Wang[3] and A. Zunger[1]

[1] *National Renewable Energy Laboratory - Golden, CO 80401, USA*
[2] *Ford Research Laboratory, MD3028/SRL - Dearborn, MI 48121-2053, USA*
[3] *Lawrence Berkeley National Laboratory - Berkeley, CA 94720, USA*

(received 21 December 2000; accepted in final form 20 April 2001)

PACS. 61.66.Dk – Alloys.
PACS. 71.15.Mb – Density functional theory, local density approximation, gradient and other corrections.
PACS. 81.30.Mh – Solid-phase precipitation.

Abstract. – We have elucidated the physical mechanisms governing the observed size- and temperature dependence of precipitate shapes in Al-Zn alloys via quantum-mechanical first-principles simulations. In remarkable quantitative agreement with alloy aging experiments, we find that with decreasing temperature and increasing average size, the precipitates change from spherical to plate-like shape. Although the precipitates are created by an inherently kinetic heat treatment process, the entire series of their size *vs.* shape relation can be explained in terms of *thermodynamic* arguments and understood in terms of strain and chemical energies.

The temperature-composition phase diagram of a solid state $A_{1-x}B_x$ alloy [1] may consist of homogeneous single-phase regions (such as ordered compounds A_mB_n, or disordered solid solutions) as well as heterogeneous, phase-coexistence regions (such as phase-separation). First-principles calculations based on the density-functional approach have been very useful in helping one to understand the stability of simple single-phased materials. This includes calculations of perfectly *ordered compounds* [2] as well as perfectly *random alloys* [3, 4], both requiring for their crystallographic description only small unit cells, containing O(10) atoms. The restriction to simple homogeneous structures leaves unexplored significant portions of the phase diagrams of many materials. Perhaps the best-known examples of heterogeneous phase-coexistence are phase separation of an alloy into its constituents [1] $A_{1-x}B_x \rightleftharpoons (1-x)A + xB$ or into a constituent plus a compound [1], *e.g.*, $A_{1-x}B_x \rightleftharpoons A_3B + A$. Such solid-state decomposition reactions create *precipitates* which define an important part of the microstructure of many alloy systems. The early stage of these reactions typically involves the formation of *coherent precipitates* that adopt the crystallographic lattice of the alloy from which they emerge [5]. Coherent precipitates have practical importance, as they act to impede dislocation motion, and thus lead to "precipitation hardening" in many alloys [5–8]. Despite their importance, precipitate microstructures were thus far not amenable to first-principles theories, since their description requires "unit cells" containing 10^3–10^5 atoms or more, well beyond current capabilities of first-principles methods.

Of particular interest are the *shapes* and *sizes* of precipitates which are found to be strongly correlated: For example, $Al_{1-x}Cu_x$ alloys exhibit a transition of coherent precipitates from {100} planes of Cu atoms to Cu-Al-Al-Al-Cu thin platelet structures [9, 10]. In $Al_{1-x}Zn_x$,

(*) Permanent address: Lehrstuhl für Festkörperphysik, Universität Erlangen-Nürnberg - Staudtstr. 7, D-91058 Erlangen, Germany. E-mail: s.mueller@fkp.physik.uni-erlangen.de

many experimental studies have been performed to examine the shapes and structure of precipitates [11–17] (due to the ability of Al-Zn to harden via precipitate heat-treatment). The Zn precipitates exhibit a remarkable series of shapes and sizes: Small precipitates tend to be spherical, until they reach a critical size $R_{\rm C}$ of about 15–25 Å (dependent on the aging temperature) at which point they become ellipsoidal/plate-like with the short axis parallel to the [111] direction. The transition radius $R_{\rm C}$ depends on temperature: it shrinks as the aging temperature is reduced. While different aging times lead to different distribution of sizes [12], remarkably, the size *vs.* shape relation is universal, irrespective of whether the aging period is minutes or weeks. In an atomistic sense, this observation raises the possibility that each individual precipitate represents locally an equilibrium configuration. Such local equilibria are a consequence of the fact that atoms in a single precipitate exchange more readily with each other than with other precipitates. Our strategy will hence be to *assume* that for Al-Zn a *thermodynamic* (rather than kinetic) description of size *vs.* shape might be appropriate, and examine the extent to which this does or does not agree with the measured distribution of sizes and shapes. We find that it does: Our calculations are quantitatively in excellent agreement with experimental results [11–17].

Prediction of precipitate size *vs.* shape requires optimization of the free-energy $F(\bar{R}, T)$ for a given average size $\bar{R}$ and temperature T with respect to all possible shapes. As we will see, in an atomistic description this requires consideration of cells containing sometimes more than 100000 atoms [18]. Many previous descriptions of precipitate shapes utilized continuum approaches in the context of empirically parametrized free-energy functionals (see, *e.g.*, refs. [7,19,20]). Here, we use an atomistic approach based on an LDA-derived cluster expansion (CE). The basic ideas are: i) to expand the energy $\Delta H_{\rm CE}(\sigma)$ of an arbitrary alloy configuration $\{\sigma\}$ as a linear sum of the energies characteristic of the underlying atomic "geometric objects" such as pairs, triangles, tetrahedra [21], ii) to determine these characteristic energies by mapping $\Delta H_{\rm CE}(\sigma_{\rm ord})$ for simple, ordered configurations onto the corresponding LDA excess energies $\Delta H_{\rm LDA}(\sigma_{\rm ord})$, and iii) to find the equilibrium precipitate shapes at finite temperatures by Monte-Carlo (MC) simulation of $\Delta H_{\rm CE}(\sigma)$ at temperatures below the coherent miscibility gap. This mixed-space cluster expansion approach (MSCE) [21] affords LDA accuracy in total energies along with a computational speed that permits detailed MC simulations (10^5 atoms/cell with 1000 spin-flips per atom and temperature) of precipitate microstructures [10, 18, 22].

In our MSCE approach [21], any configuration σ is defined by specifying the occupations of each of the N lattice sites by an Al atom (spin-index $\hat{S}_i = -1$) or a Zn atom ($\hat{S}_i = +1$). The formation enthalpy of any configuration σ at its atomically relaxed state is then given by

$$\Delta H_{\rm CE}(\sigma) = \sum_{\boldsymbol{k}} J_{\rm pair}(\boldsymbol{k}) |S(\boldsymbol{k},\sigma)|^2 + \sum_{f}^{MB} D_f J_f \bar{\Pi}_f(\sigma) + \frac{1}{4x-1} \sum_{\boldsymbol{k}} \Delta E^{\rm eq}_{\rm CS}(\hat{k}, x) |S(\boldsymbol{k},\sigma)|^2 \,. \quad (1)$$

The first two terms represent the *chemical energy*, $E_{\rm chem}$ (often refered to as *interfacial energy*). Here, the first sum describes all possible pair figures. $J_{\rm pair}(\boldsymbol{k})$ is the lattice Fourier transform of the real space pair interactions, and $S(\boldsymbol{k},\sigma)$ are structure factors. The second sum describes many-body figures, such as triangles, tetrahedra, etc. Here, J_f is the real-space effective many-body interaction of figure f, D_f stands for the number of equivalent clusters per lattice site and $\bar{\Pi}_f(\sigma)$ are spin products. The third term, the *constituent strain*, $E_{\rm CS}$ (often referred to as *coherency strain*), describes the strain energy necessary to maintain coherency between bulk Al and fcc Zn along an interface with orientation $\hat{k}$. It can be calculated by deforming the bulk elements (Al and fcc-Zn) from their equilibrium lattice constants $a_{\rm Al}$ and $a_{\rm Zn}$ to a common lattice constant a perpendicular to $\hat{k}$. The constituent strain is a function of composition x and direction $\hat{k}$ only, but does not include information about the strength

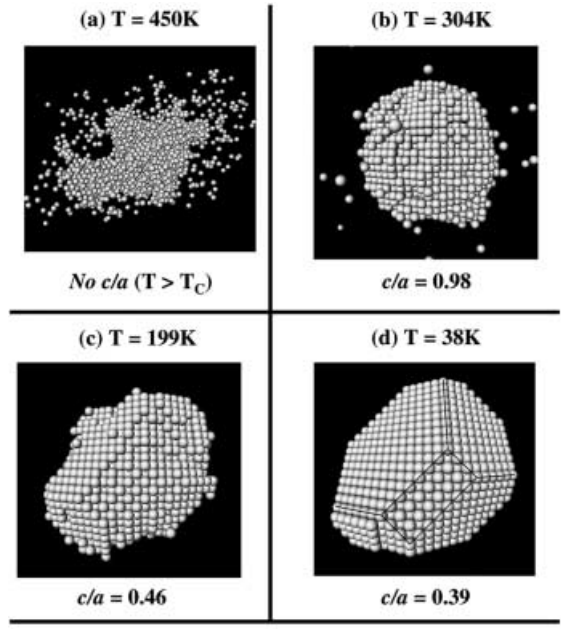

Fig. 1 – Shape *vs.* temperature of a Zn precipitate in the $Al_{24825}Zn_{2175}$ alloy. Only Zn atoms are shown. With decreasing temperature, the shape changes from a nearly spherical (large c/a) to a more plate-like (small c/a) form.

of chemical interactions between Al and Zn atoms.

We determine $\{J_{\rm pair}(\boldsymbol{k})\}$ and $\{J_f\}$ by fitting $\Delta H_{\rm CE}(\sigma_{\rm ord})$ to a set of 26 ordered (ord) Al_nZn_m compounds. The sets $\{\sigma_{\rm ord}\}$ includes (among others) superlattices of ten different Zn-compositions five different layer orientations. These formation enthalpies are calculated within the LDA as implemented by the pseudopotential plane-wave method [23]. Comparing $\Delta H_{\rm CE}$ to $\Delta H_{\rm LDA}$ for 9 ordered Al-Zn compounds *which were not used in the construction* of $\{J_{\rm pair}(\boldsymbol{k})\}$ and $\{J_f\}$ shows an "average prediction error" of only 2 meV/atom [24]. This precision requires inclusion of up to 20 pair interactions.

To calculate equilibrium shapes of coherent precipitates we use $\Delta H_{\rm CE}(\sigma)$ of eq. (1) in canonical ensemble MC simulations. In order to exclude boundary effects, unit cells containing up to 216000 atoms were needed for the largest precipitates. The MC annealing process is initialized at a sufficiently high temperature, where the solid solution is thermodynamically stable. Using a given number $N_{\rm Zn}$ of Zn atoms in the MC cell (hence, a given average precipitate size $\bar{R}$), the system is carefully annealed below the coherent fcc miscibility gap. Upon crossing this solvus, a coherent precipitate is formed (fig. 1(a) and (b)). The MC cell size and number of spin flips are increased until the precipitate shape remains unchanged. At this point we record the shape obtained for a given average size $\bar{R} = (ca^2)^{1/3}$ and temperature T. The shape is measured by the ratio c/a between the short (c) and the two long (a) axes of the precipitate.

Figure 1 shows the calculated equilibrium shape of an $Al_{24825}Zn_{2175}$ supercell as a function of its aging temperature. For clarity, only the Zn atoms are displayed in the figures of the present paper([1]). The phase boundary between solid solution (fig. 1(a)) and coherent

([1])Note that due to perspective view, one might misinterpret some of the shapes shown in figs. 1 and 2. For instance, the shape in fig. 2(d) is *plate-like*, not *needle-like*.

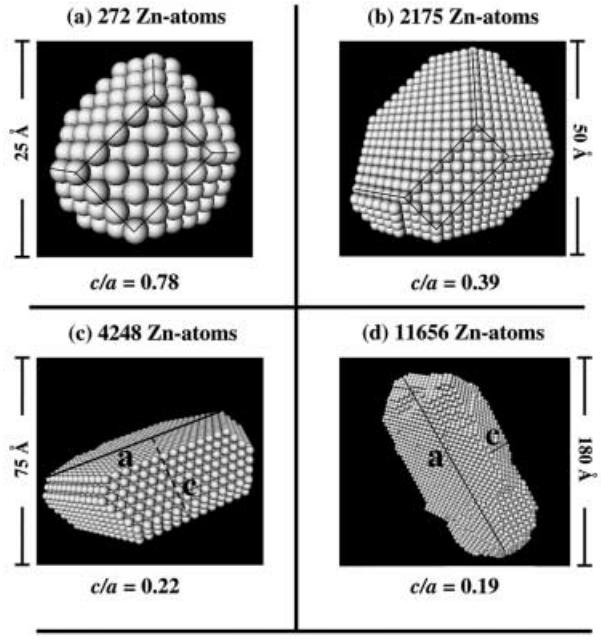

Fig. 2 – Dependence of the precipitate shape on its size (given by the number of Zn atoms) for $T \to 0$. Only Zn atoms are shown. With increasing size, the shape changes from a nearly spherical (larger c/a) to a more plate-like form (smaller c/a).

precipitate (fig. 1(b)) is calculated to be $T_c = 360$ K at this composition. We see that above T_c at $T = 450$ K there is a disordered phase, but Zn begins to precipitate once we lower the temperature below T_c. Figure 2 shows the low-temperature limit of the equilibrium shapes for various precipitate sizes (MC cell sizes: 27 000–216 000 sites). We see from fig. 1 and 2 that 1) for a given number of Zn atoms the precipitate becomes flatter (smaller c/a) with decreasing temperature. At low temperatures the precipitates show faceting with [111] facets; 2) with increasing number of Zn atoms, the precipitate shape changes from a nearly spherical ($c/a \approx 1$) into a more plate-like shape; 3) precipitates flatten in the [111] direction (fig. 1(d)). To critically assess these results quantitatively, fig. 3 compares the measured [11,13,15–17] and calculated precipitate shapes (c/a) for two different temperatures. The experimental values correspond to $Al_{1-x}Zn_x$ alloys with $x = 0.068$ and $x = 0.138$ for $T = 300$ K and $T = 200$ K, respectively. Our quantum-mechanical predictions were done for *exactly* these two concentrations and temperatures. The agreement is excellent: Our thermodynamic theory accounts quantitatively for the change of c/a ratio with size and temperature. For samples aged at room temperature the shape c/a is nearly 1 up to about $r_m = 2$ nm. Then, the c/a-ratio starts to decrease until it reaches a value of about 0.3 at $r_m = 6$ nm. For a given size r_m, c/a can only be changed by lowering the aging temperature: The lower the aging temperature the smaller is the resulting c/a ratio. We conclude that although the precipitates are created by an inherently kinetic heat treatment process, the entire series of their size *vs.* shape relation can be explained in terms of *thermodynamic* arguments. Furthermore, first-principles theory can *predict* the size *vs.* shape relation within experimental accuracy.

To understand the physical contributions which give rise to points 1)-3) above, we analyze the shapes obtained in our simulation by using the partitioning of the cluster expansion

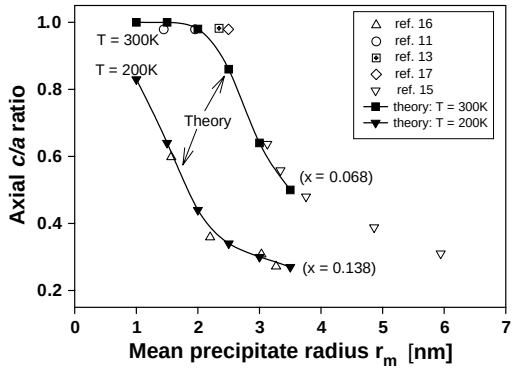

Fig. 3 – Shape (c/a) *vs.* size relation of Zn precipitates for two different temperatures. The mean precipitate redius $r_{\rm m}$ is given by $r_{\rm m} = (ca^2)^{1/3}$. The lines denote the results from our calculations, the open points are taken from different experimental studies [11, 13, 15–17].

Hamitonian, eq. (1), into chemical energy, $E_{\rm chem}$, and constituent strain energy, $E_{\rm CS}$. We annealed again the $Al_{24825}Zn_{2175}$ supercell (used for the temperature study in fig. 1), but this time instead of using the *full* Hamiltonian in the MC simulation we used only a) the constituent strain energy $E_{\rm CS}$, and separately b) the chemical energy $E_{\rm chem}$. a) Using only the strain part $E_{\rm CS}$ in the simulation gives platelet-stabilization with $c/a \to 0$. As expected, the direction of the platelet is the elastically softest direction of the precipitate [7, 18–20]. The soft direction for coherency strain is [111], not the [100] direction common for fcc lattice, even though [100] is the softest direction for bulk elastic strain in Al-Zn alloys [25, 26]. The reason is the following: Zn is naturally an hcp element, but in Al-rich $Al_{1-x}Zn_x$ alloys, it is forced to have the fcc structure of the alloy. It thus develops an instability [24] in the form of an anomalously low energy for the [111]-deformed unit cell. As a consequence, [111] is the elastically softest direction of fcc-Zn, resulting in extremely small (< 1 meV/atom) coherency strain energies along this direction. This [111]-soft precipitates are embedded in a matrix of Al which has an elastically soft [100] direction. While the [100] softness of Al has been shown to yield spinodal decomposition fluctuations along this direction [27], it does not control the plate orientation of (relatively) large Zn precipitates due to the well-known result of Khachaturyan [7] that the habit plane of a precipitate is determined by the elastic constants of the precipitate phase, and *not* by those of the matrix. So, for Zn-rich alloys, the constituent strain would be dictated by the elastic response of Al, and hence would become more and more isotropic. b) Using only the "chemical part" $E_{\rm chem}$ leads to a compact, but *faceted* polyhedron. The interfaces are oriented in the four [111] directions. This faceting caused by the chemical part of the Hamiltonian is a consequence of a strong anisotropy of the chemical energy for Al-Zn. This chemical anisotropy is evident from the fact [24] that [111] oriented Al_n/Zn_n superlattices have much lower chemical energies than superlattices in other orientation.

In order to study quantitatively the importance of $E_{\rm chem}$ and $E_{\rm CS}$, we calculated them for different *assumed* (*i.e.* not annealed by Monte Carlo) precipitate shapes, such as spheres and hexagonal plates as well as flat [111] layers and random alloys. The resulting values for $E_{\rm chem}$ and $E_{\rm CS}$ are collected in fig. 4. We see from fig. 4 that:

a) In the range $0.35 < c/a < 1$ the strain energy $E_{\rm CS}$ depends only weakly on c/a. Only for the ideal [111] layers ($c/a \to 0$) is $E_{\rm CS}$ characteristically lower than for all other shapes.

b) On the other hand, $E_{\rm chem}$ decreases significantly with decreasing c/a ratio even though the interfacial area increases. For examples for ~ 300 Zn atoms (energies are given in meV/Zn

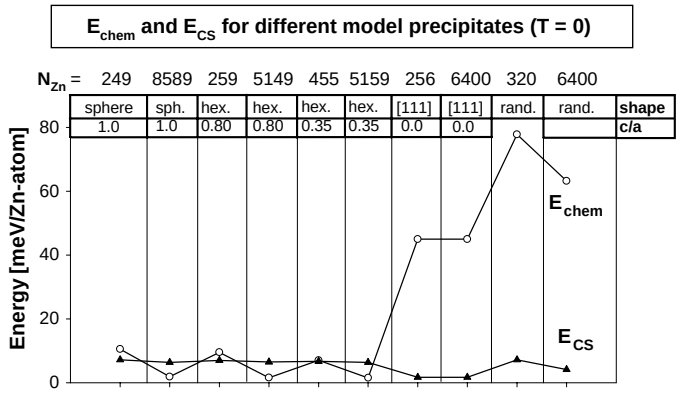

Fig. 4 – Chemical energy, $E_{\rm chem}$, and constituent strain energy, $E_{\rm CS}$ for different precipitate models with different shapes and sizes. While $E_{\rm CS}$ is nearly structure independent, $E_{\rm chem}$ shows a size- and shape dependence.

atom), $E_{\rm chem}$ is 10.5, 9.5, 7.0 for $c/a = 1$, 0.8, 0.35, respectively. This is a consequence of an unusually strong anisotropy of the chemical energy in Al-Zn.

c) $E_{\rm chem}$ decreases as the precipitate size increases since the surface-to-volume ratio increases.

The conventional understanding (see, *e.g.*, [7]) of spherical *vs.* plate-like precipitate shapes is based on the balance between strain and interfacial (chemical) energies: As precipitates get larger, strain energies dominate over chemical energies, and lead to plate-like shapes along the elastically soft direction. For small precipitates, chemical energies can dominate, and hence lead to spherical shapes which minimize interfacial area. Although this view is certainly correct in cases where the chemical energies are isotropic, we find here that Al-Zn shows an extremely large anisotropy of the chemical energy which plays an important role in shapes of Zn precipitates, particulary in the extent to which the precipitate facet at low temperatures: The anisotropy of the chemical energy depends on temperature. At low T, when entropy is unimportant, only energy-minimizing configurations emerge. Thus, the anisotropy of chemical energy is exposed at its maximum at low T. In contrast at high T, where many configurations coexist due to entropy, the chemical anisotropy is largely averaged out. Although one might qualitatively expect [111] faceting intuitively (since these interfaces are close-packed), we find that the large, unexpected anisotropy of $E_{\rm chem}$ leads to quantitatively large [111] facets.

We can now explain the observations 1)-3) we deduced from fig. 3:

1) At low T, the strong anisotropy of the chemical energy creates facets along planes of low interfacial energy. Indeed, the calculations of figs. 1 and 2 demonstrate the energetic preference for [111] facets. However, the chemical part alone, while stabilizing facets, still leads to $c/a = 1$ (as shown by Herring [28], the equilibrium shape obtained from pure chemical interaction is determined by the Wulff construction which does not allow flattening). Indeed, only $E_{\rm CS}$ can produce $c/a < 1$. Thus, the equilibrium c/a value at $T \to 0$ is dictated by the competition between $E_{\rm chem}$ (driving $c/a \to 1$) and $E_{\rm CS}$ (driving $c/a \to 0$). Figure 4 shows that the magnitudes of $E_{\rm CS}$ and $E_{\rm chem}$ alternate, being connected thus to different c/a values. At high temperatures, where the chemical anisotropy diminishes, we observe *spherical* precipitates, exactly as found in earlier theoretical studies that assumed simplified, *isotropic* chemical terms [20]. This explains why as the temperature decreases we find a spherical-to-faceted shape transition.

2) As the number N_{Zn} of Zn-atoms increases, c/a decreases since the variation of strain energy with shape is smaller (point a) above) than the variation of the chemical energy with shape (point b) above).

3) Precipitates flatten in the [111] direction since both the elastic instability of fcc Zn and the chemical anisotropy of Al-Zn happens to occur along [111].

One might think that the use of continuum elasticity plus empirical interfacial energies might have sufficed to study precipitate shapes in Al-Zn. However, our work shows effects that are unsuspected, such as the large anisotropy of the interfacial energies and the critical role of the elastic constants of an unstable phase: fcc-Zn. Our approach provides both, quantitative predictions as well as a microscopic picture for the variations in shape and size with temperature, supporting the view that thermodynamic, rather than kinetic explanations are sufficient for describing precipitate shapes in Al-Zn.

* * *

The work at NREL was supported by the Office of Science, Basic Energy Science, Material Science Division, U.S. Department of Energy under Contract No. DE-AC36-99-GO10337.

REFERENCES

[1] Villars P. and Calvert L. D., *Pearson's Handbook of Crystallographic Data* (ASM International, Materials Park) 1991.
[2] Fernando G. W., Watson R. E. and Weinert M., *Phys. Rev. B*, **45** (1992) 8233.
[3] Johnson D. D., Nicholson D. M., Pinski F. J., Gyorffy B. L. and Stocks G. M., *Phys. Rev. Lett.*, **56** (1986) 2088.
[4] Zunger A., Wei S.-H., Ferreira L. G. and Bernard J. E., *Phys. Rev. Lett.*, **65** (1990) 353.
[5] Guinier A., *Solid State Phys.*, **9** (1959) 293.
[6] Cohen J. B., *Solid State Phys.*, **39** (1986) 131.
[7] Khachaturyan A. G., *Theory of Structural Transformations in Solids* (John Wiley, New York) 1983.
[8] Zandberger H. W., Andersen S. J. and Jansen J., *Science*, **277** (1997) 1221.
[9] Gerold V. (Editor), *Viewpoint Set Scripta Metall.*, **22** (1988) 927.
[10] Wolverton C., *Philos. Mag. Lett.*, **79** (1999) 683.
[11] Laslaz G. and Guyot P., *Acta Metall.*, **25** (1977) 277.
[12] Ramlau R. and Löffler H., *Phys. Status Solidi A*, **79** (1983) 141.
[13] Bubeck E., Gerold V. and Kostorz G., *Cryst. Res. Technol.* **20** (1985) 97.
[14] Hübner G., Löffler H. and Wendrock G., *Cryst. Res. Technol.* **21** (1986) 8.
[15] Fumeron M., Guillot J. P., Dauger A. P. and Caisso J., *Scripta Metall.*, **14** (1980) 189.
[16] Deguercy J., Denanot M. F., Fumeron M., Guillot J. P. and Caisso J., *Acta Mater.*, **30** (1982) 1921.
[17] Gerold V., Siebke W. and Tempus G., *Phys. Status Solidi A*, **104** (1987) 213.
[18] Wolverton C., *Model. Simul. Mat. Sci.*, **8** (2000) 323.
[19] Thompson M. E., Su C. S. and Voorhees P. W., *Acta Met. Mater.*, **42** (1994) 2107.
[20] Lee J. K., Barnett D. M. and Aaronson H. I., *Met. Trans. A*, **8** (1977) 963.
[21] Zunger A., *NATO ASI* on *Statics and Dynamics of Alloy Phase Transformations*, edited by Turchi P. E. A. and Gonis A. (Plenum Press, New York) 1994, p. 361.
[22] Asta M. and Hoyt J. J., *Acta Mater.*, **48** (2000) 1089.
[23] Ihm J., Zunger A. and Cohen M. L., *J. Phys. C*, **12** (1979) 4409.
[24] Müller S., Wang L.-W., Zunger A. and Wolverton C., *Phys. Rev. B*, **60** (1999) 16448.
[25] Guilarducci de Salva A., Simon J. P., Livet F. and Guyot P., *Scripta Met.*, **21** (1987) 1061.
[26] Ujihara T., Osamura K. and Amemiya Y., *J. Jap. Inst. Met.*, **62** (1998) 117.
[27] Cahn J. W., *Acta Metall.*, **10** (1962) 179.
[28] Herring C., in *Structure and Properties of Solid Surfaces*, edited by Gomer R. and Smith C. S. (University of Chicago Press, Chicago) 1953, p. 5.